Layer-by-layer-assembled chitosan/phosphorylated cellulose nanofibrils as a bio-based and flame protecting nano-exoskeleton on PU foams

Layer by Layer-Assembled Chitosan/ Phosphorylated Cellulose Nanofibrils as a Bio-based and Flame Protecting Nano-exoskeleton on PU foams

F. Carosio[*1], *M. Ghanadpour* [2], *J. Alongi*[3], *L. Wågberg* [2,4]

[1]Dipartimento di Scienza Applicata e Tecnologia, Politecnico di Torino, Alessandria campus, Viale Teresa Michel 5, 15121 Alessandria, Italy

[2]Department of Fiber and Polymer Technology, KTH Royal Institute of Technology, SE-100 44 Stockholm, Sweden

[3]Dipartimento di Chimica, Università degli Studi di Milano, Via Golgi 19, 20133 Milano, Italy

[4]Wallenberg Wood Science Center at the Department of Fiber and Polymer Technology, KTH Royal Institute of Technology, SE-100 44 Stockholm, Sweden

* Tel.: +39 0131 229303, Fax: +39 0131 229399 E-mail: federico.carosio@polito.it

e-mail addresses: marygp@kth.se (M. Ghanadpour), jenny.alongi@unimi.it (J. Alongi), wagberg@kth.se (L. Wågberg)

Abstract

The layer-by-layer (LbL) assembly of chitosan (CH) and phosphorylated cellulose nanofibrils (P-CNF) is presented as a novel, sustainable and efficient fire protection system for polyurethane foams. The assembly yields a linearly growing coating where P-CNF is the main component and is embedded in a continuous CH matrix. This CH/P-CNF system homogenously coats the complex 3D structure of the foam producing a nano-exoskeleton that displays excellent mechanical properties increasing the modulus of the foam while maintaining its ability of being cyclically deformed. During combustion the CH/P-CNF exoskeleton efficiently prevents foam collapse and suppresses melt dripping while reducing the heat release rate peak by 31% with only 8% of added weight. The coating behavior during combustion is investigated and correlated to the observed performances. Physical and chemical mechanisms are identified and related to the unique composition and structure of the coating imparted by the LbL assembly.

KEYWORDS: layer by layer; chitosan; phosphorylated cellulose nanofibril; polyurethane foams; thermal stability; flame retardancy

INTRODUCTION

In recent years, the scientific community has focused significant efforts on the use of bio-based resources for the production of functional materials capable of meeting current societal demands for green and sustainable alternatives. The fire protection of materials represents an area of great concern. Indeed, due to recently perceived environmental problems, some of the currently adopted chemicals and treatments (defined flame retardants) have been under regulatory scrutiny and subsequently either banned or strongly limited in their applications. (Stieger, Scheringer, Ng, & Hungerbuhler, 2014) This situation creates a strong demand for new, high performing and environmentally friendly fire protection solutions. Recently, it has been demonstrated that deoxyribonucleic acid (DNA) extracted as by-product from fish production can be employed to deliver efficient flame retardant solutions. (J. Alongi, Carletto, et al., 2013) (J. Alongi, Di Blasio, Cuttica, Carosio, & Malucelli, 2014) (Carosio, Cuttica, Di Blasio, Alongi, & Malucelli, 2015) (Jenny Alongi, Cuttica, & Carosio, 2016). Beside DNA, nature can offer other bio-based building blocks such as chitosan and nanofibrillated cellulose (CNF) that are characterized by a much larger availability and sustainability. Indeed, chitosan can be produced by deacetylation of chitin extracted from crab shells while CNF can be conveniently extracted from wood fibers, or other cellulose containing materials, yielding fibrils with typical dimensions of 3-15 nm in diameter and 0.7-3 micrometers in length. (Dash, Chiellini, Ottenbrite, & Chiellini, 2011) (Klemm et al., 2011) CNF represents one of the newest and most interesting bio-based building blocks for material preparation and it is currently studied in a wide variety of application fields.(Lavoine, Desloges, Dufresne, & Bras, 2012) (Jorfi & Foster, 2015) (Du, Zhang, Liu, & Deng, 2017) Both chitosan and CNF possess interesting key features that make them appealing for the construction of functional flame resistant materials. For instance, chitosan has been employed as cationic polyelectrolyte for the layer-by-layer (LbL) assembly of highly flame retardant and nanostructured thin films. (Leistner, Abu-Odeh, Rohmer, & Grunlan, 2015) (Cain et al., 2014) (Carosio & Alongi, 2016b) (Koklukaya, Carosio, & Wãgberg, 2017) This technique simply consists in the alternate adsorption of chemical species on a

substrate on the basis of both specific and nonspecific interaction (e.g. electrostatic attraction between polyions and/or nanoparticles) yielding stratified or highly interpenetrated nanostructured coatings. (Decher, 1997) On the other hand, water-based CNF colloids have been processed using simple paper-making approaches to produce nanostructured films with peculiar mechanical and physical properties including optical transparency, gas barrier properties and flame retardancy characteristics. (Henriksson, Berglund, Isaksson, Lindstrom, & Nishino, 2008) (Liu & Berglund, 2012) (Carosio, Kochumalayil, Cuttica, Camino, & Berglund, 2015) Recently, we have reported the preparation of phosphorylated cellulose nanofibrils (P-CNF): an inherently flame retardant version of CNF that can be used in water-based processes to prepare strong nanosheets with self-extinguishing and non-ignitability properties. (Ghanadpour, Carosio, Larsson, & Wagberg, 2015)

In this paper we are applying the LbL assembly of chitosan and P-CNF for the production of nanostructured fire shielding thin films capable of protecting dense (100 g/dm^3) open cell polyurethane foams (PU). PU foams are often referred to as the principal cause for fire initiation and spreading to other materials due to melt dripping and hence represent a substrate in strong need for novel and efficient fire protection solutions. (Hirschler, 2008) (Hammel et al., 2017) (Cho et al., 2015) (Xu, Yu, & Qian, 2017) The study of this CH/P-CNF assembly as well as its application to PU foams has never been reported before and represents a novel example of a fully renewable and nature-based FR solution. The LbL assembly poses further advantages with respect to conventional approaches allowing for the use of a green and sustainable technique that operates with diluted water-based suspension/solution at room conditions under pHs between 4 and 9. Figure 1 shows a schematic representation of the approach proposed in this paper.

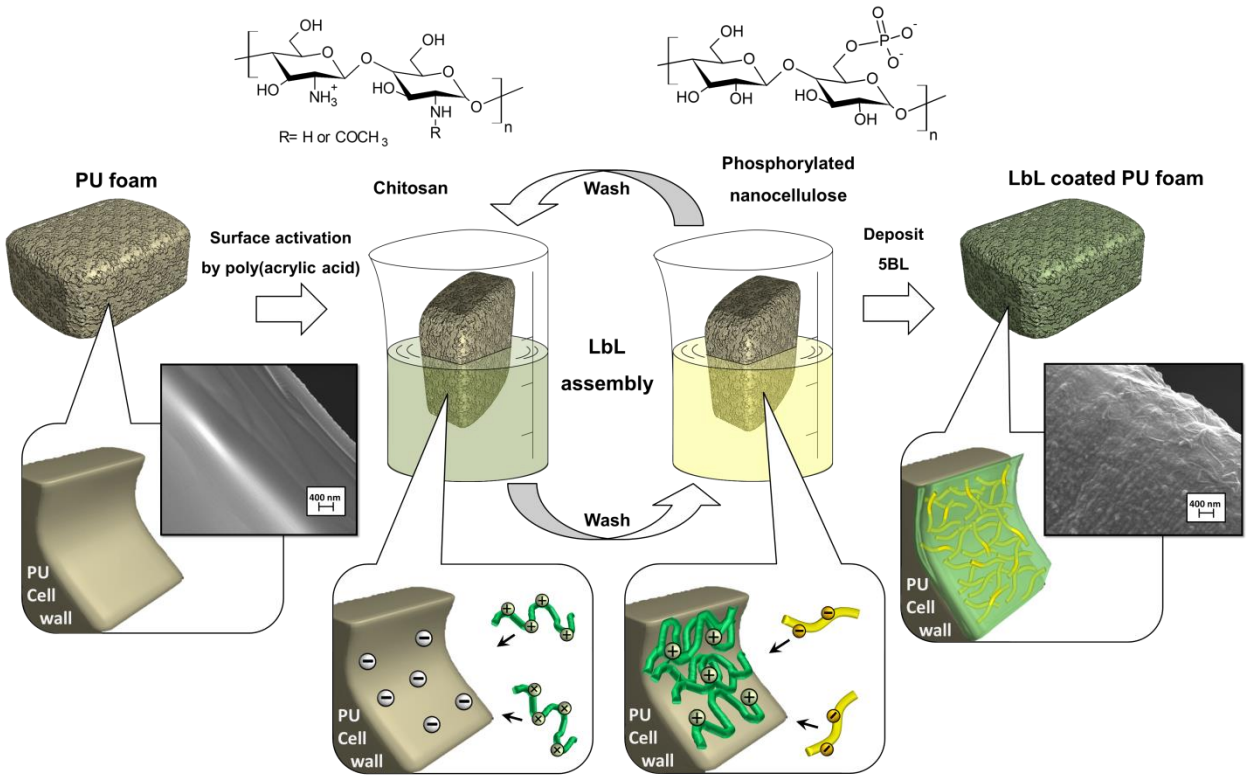

Figure 1. Schematic representation of the LbL process exploited in this manuscript. PU foams are pre-activated by poly(acrylic acid) and then alternatively dipped in the chitosan (positive) and phosphorylated cellulose nanofibrils (negative) baths. The process is repeated 5 times in order to deposit 5 Bi-Layers (BL). (Note that the components in the images are not drawn to scale).

The LbL assembly of CH and P-CNF has been evaluated by investigating the coating composition and morphology. The hypothesis is that the LbL allows for unique compositional and structural features that subsequently result in synergistic rather than additive interactions between the chitosan and P-CNF. CH can act as the continuous matrix embedding the anionic P-CNF which can enhance the coating char formation, during combustion, allowing for the production of protective thermally stable carbonaceous structures. (Carosio, Alongi, & Malucelli, 2012) To verify this, the LbL assembled CH/P-CNF coating has been studied as a standalone material evaluating its thermal and thermo-oxidative stability as well as the structural and chemical changes resulting from the exposure to a heat source. The achieved results have then been related to the coating performances on foams. The approach developed in this paper allows for a better understanding of the

structure/property relationship in FR-LbL assemblies and poses the base for the design of more efficient FR solutions consisting of sustainable resources

2. Experimental Details

2.1 Materials: open cell polyurethane foams (PU) (100 g/dm^3, thickness of 15 mm) have been supplied by Compart (France). Poly(acrylic acid) (average Mw ~100000, 35 wt. % in H_2O), branched poly(ethylene imine) (BPEI, Mw ~25,000 by Laser Scattering, Mn ~10,000 by Gel Permeation Chromatography, as reported in the material datasheet), were purchased from Sigma Aldrich (Milwaukee, WI). Chitosan (CH, Mw ~ 60,000, 95% deacetylation) was purchased from GTC Union Corp., Qingdao, China. Poly(diallyldimethylammonium chloride) (PDADMAC, solution, Mw 400,000 - 500,000, 50 wt.% in H_2O) was purchased from Sigma Aldrich. The polymer was purified by dialysis followed by freeze-drying prior to use. Poly(vinylsulfate potassium) (KPVS colloidal titration grade, solution, Mw of the repeating unit 162.21, N/400 in H_2O) was purchased from Wako Pure Chemical Industries, Ltd. and diluted with Milli-Q water prior to use The P-CNF gel used in this work was obtained from the phosphoryl functionalized fibers based on a previously described procedure. (Ghanadpour et al., 2015) The P-CNF dispersion to be used in LbL assembly was prepared by diluting a 2 wt.% gel in Milli-Q water followed by ultra-sonication for 10 min at 40% amplitude using a Sonics & Materials, Inc. Vibra-cell equipped with a titanium probe. The aggregated and non-fibrillated fiber fragments were then removed by centrifugation at 4,500 rpm for 1 h and the supernatant was collected as the stable P-CNF dispersion. PAA was employed as 1 wt.-% water solution, while BPEI, CH, P-CNF were used at 0.1 wt.-%. The water employed was a 18.2 MΩ deionized water supplied by a Q20 Millipore system (Milano, Italy). The pH of PAA and BPEI were used at their unmodified pH of 3 and 10, respectively. CH was firstly dissolved at pH 2 and then pH was adjusted to 5. The ionic strength of the solution was changed by adding 10 mM NaCl. The pH of the P-CNF suspension was adjusted to 6. Solutions of 2M HCl and 1M NaOH were employed to adjust the pH.

2.2 Layer by Layer deposition on Si Wafers: before LbL deposition, the surface of Si wafers was activated by 5 min dipping in a 0.1 wt.-% BPEI solution, washed with deionized water and dried with compressed air. Then, the Si wafer was alternately dipped into the P-CNF and CH solutions in order to deposit one bi-layer repetitive unit. The deposition time was set to 15 min for P-CNF and 10 min for CH. After each adsorption step the silicon wafer was washed with deionized water. An automatic dipping robot (StratoSequence VI, nanoStrata Inc., Tallahassee, FL, USA) was used to fabricate a 150BL film for structural and post combustion analyses.

2.3 Layer by layer deposition on PU foams: before the deposition, the foams were dipped and squeezed in deionized water in order to remove dust and residual cell walls and then dried in an oven (80°C). Then, the foams were firstly dipped in 1 wt.-% PAA solution with pH 3 for 10 min. Following this activation step, the foams were alternately dipped in the CH and P-CNF solution until 5 BL were formed. The dipping time for CH was set to 10 min whereas it was increased to 15 min for P-CNF. After each deposition step, the foams were carefully squeezed and washed by dipping in deionized water for 5 min. At the end of the process, the treated foams were dried in an oven at 80°C.

2.4 Characterization

Fourier transformed-infrared spectroscopy (FT-IR): the growth of the LbL assembly was monitored using a Frontier FT-IR/FIR spectrophotometer (16 scans and 4 cm^{-1} resolution, Perkin Elmer, Milano, Italy). IR spectra were acquired, at room temperature, after each deposition step.

Fourier transformed-infrared spectroscopy in attenuated total reflectance (FT-IR ATR): spectra in the range 4000-700cm^{-1} (16 scans and 4cm^{-1} resolution) were collected at room temperature using a FT-IR/FIR spectrophotometer (Perkin Elmer mod. Frontier, Waltham, MA, USA) equipped with a diamond crystal.

Raman spectroscopy: raman spectra were performed on a InVia Raman Microscope (Renishaw, argon laser source 514 nm/50mW, 10 scans) coupled with a Leica DM 2500 optical microscope.

Quartz crystal microbalance with dissipation (QCM-D): the LbL build-up of the CH/P-CNF assembly was also monitored by QCM-D (E4, Q-Sense AB, Västra Frölunda, Sweden) using a method described in detail elsewhere. (Rodahl, Höök, Krozer, Brzezinski, & Kasemo, 1995) The AT-cut quartz crystal sensors with silicon oxide coating were also purchased from Q-Sense AB and were plasma cleaned for 2 min at 30 W, immediately before use. This QCM-D technique allows for simultaneous measurement of the change in resonance frequency (Δf) and energy dissipation (D) of the QCM crystal upon adsorption to the crystal surface. The normalized frequency change is directly proportional to the sensed mass, which corresponds to both the adsorbed species and the associated water, according to the Sauerbey relation:

$$\Delta m = C\Delta f / n \qquad \text{Eq. 1}$$

where Δm is the change in the adsorbed mass per area, C is the mass sensitivity constant (-0.177 mg/m^{2}Hz), Δf is the change in frequency and n is the number of the overtone. The energy dissipation can be related to the viscoelastic properties of the adsorbed layer.(Aulin, Varga, Claesson, Wågberg, & Lindström, 2008)

Polyelectrolyte titration: the amount of CH and P-CNF adsorbed onto the PU foam in each layer deposition was determined by polyelectrolyte titration of the residual CH or P-CNF in the solution after the adsorption. A combination of a Metrohm 716 DMS Titrino titrator and a Particle Metrix Stabino stability analysis system was used, where CH was titrated by negatively charged polyvinylsulfate potassium (KPVS) and P-CNF was titrated by positively charged polydiallyldimethylammonium chloride (PDADMAC).

Field Emission-Scanning Electron Microscopy (FE-SEM): surface morphology of untreated and LbL treated foams was investigated using a Field Emission-Scanning Electron Microscopy ZEISS, FEG model MERLIN (beam voltage: . The cross section of Si wafers was obtained by fragile fracture of the substrates, while untreated and LbL treated foams were cut in small pieces (10 x 10 x 5 mm^3). The resulting samples were placed on conductive adhesive tapes and chromium-metallized.

Thermogravimetric analysis (TGA): thermogravimetric analysis under nitrogen atmosphere (gas fluxes of 60 and 40 ml/min for sample gas and balance protection gas, respectively) was performed by a TAQ500 of Waters-TA Instruments (Milano, Italy). The sample (approx. 10 ± 0.5 mg) was placed in open alumina pans and heated from 50 to 800°C using a heating rate of 10°C/min. $T_{onset10\%}$ (temperature at 10% of weight loss), T_{max} (temperature at maximum rate of weight loss), and residue at 800°C were obtained by these measurements.

Mechanical properties: compression stress/strain measurements were performed with approximately 1 cm^3 untreated and LbL-coated PU foams, using the Instron 5944 (Instron Corporation, High Wycombe, UK) instrument equipped with a 500 N load cell. The foam samples were cyclically compressed between two metallic plates up to 90% strain, using a strain rate of 10 %/min during the three applied cycles. The samples were conditioned prior to the test at 23 °C and 50% R.H. and the test was repeated at least 5 times for each formulation in order to ensure reproducibility.

Flammability: the flammability of prepared samples has been tested in horizontal configuration following the ASTM D 4986 standard. The sample (30 x 100 x 15 mm^3) was positioned on a metallic grid and ignited from its short side by a 20 mm blue methane flame (flame application time: 6 s). Dry cotton wad was placed 30 cm underneath the metallic grid in order to evaluate the occurrence of the melt dripping phenomenon. Each test was repeated 3 times for each formulation in order to ensure reproducibility; during the test, parameters such as burning rate, final residue and formation of incandescent droplets of molten polymer were registered.

Cone calorimetry: cone calorimetry (Fire Testing Technology, FTT, UK) was employed to investigate the combustion behavior of untreated and LbL-treated foams (50 x 50 x 15 mm^3) under 35kW/m^2 in horizontal configuration, following the ISO 5660 standard. The following parameters were registered: Time To Ignition (TTI, [s]), peak of Heat Release Rate (pkHRR, [kW/m^2]), Total Heat Release (THR, [MJ/m^2]), and final residue (%). Before flammability and cone calorimetry tests, samples were conditioned for at least 24 hours in a climatic chamber (23°C, 50% R.H.)

3. Results and discussion

3.1 Coating growth by FT-IR spectroscopy and QCM-D using SiO_2 surfaces

Each layer constituent has been firstly evaluated by FT-IR spectroscopy (*see* Figure S1 in Supporting Information). Neat chitosan shows characteristic signals related to NH_3^+ asymmetric (1624 cm^{-1}) and symmetric (1522 cm^{-1}) stretching, C-O-C stretching of the glyosidic linkage at 1090 cm^{-1} and CH_2 groups (1450-1300 cm^{-1}). (Socrates, 2006) Similar to CH, the most intense peak of pure P-CNF is ascribed to C-O-C groups from glycosidic units or from β-(1→4)-glycosidic bonds (1060 cm^{-1}); the presence of the phosphate functionalization is highlighted by minor peaks/shoulders associated to P-O (966 and 928 cm^{-1}) and P=O (1234 cm^{-1}) groups.(Ghanadpour et al., 2015) (Socrates, 2006) The layer by layer growth of CH and P-CNF can be easily followed by IR spectroscopy, as reported in Figures 2 a, 2 b and 2 c displaying the 3D projection of the restricted IR regions and the intensity of the peak at 1060 cm^{-1} plotted as a function of BL number.

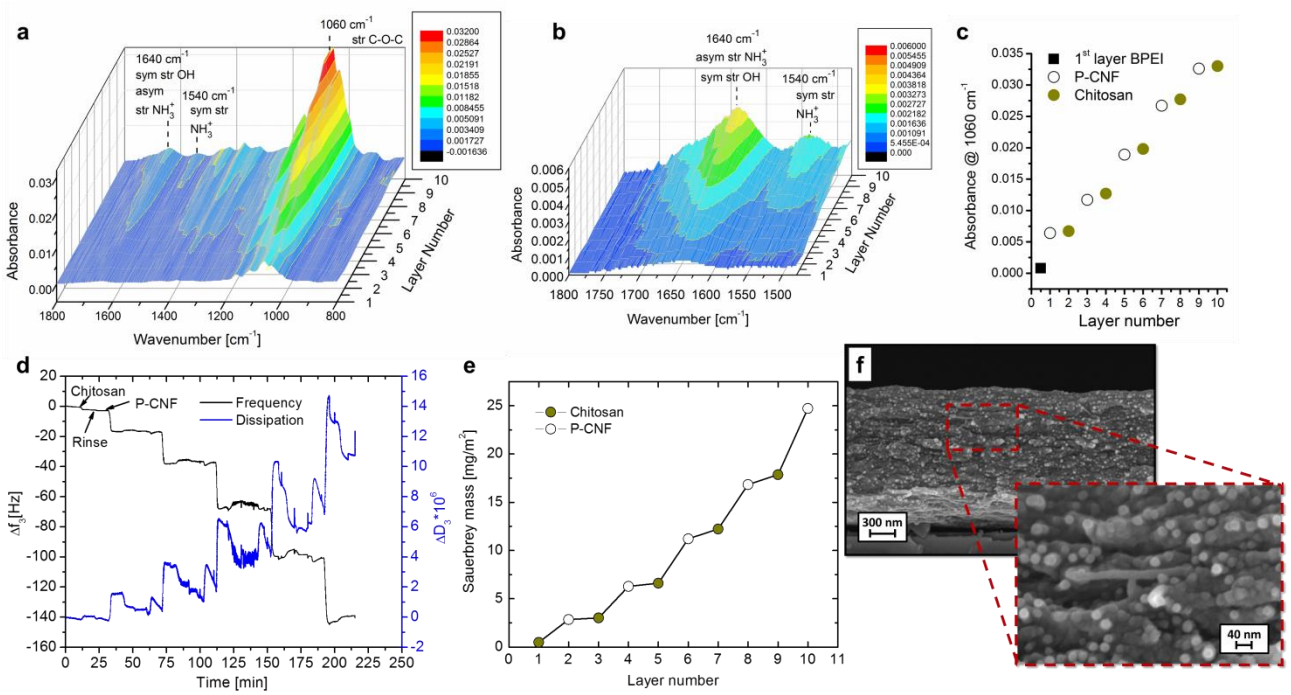

Figure 2. Characterization of the build-up of CH/P-CNF assembled on SiO_2 surfaces by using IR and QCM: (a) and (b) 3D projection of restricted IR region, (c) intensity of the IR signal at 1060

223 cm^{-1} as function of deposited BL number, (d) change in normalized frequency and energy
224 dissipation through the multilayer build-up, (e) total adsorbed mass of multilayer film calculated
225 using the Sauerbrey model and (f) FE-SEM micrographs of Si wafer cross section of the coating at
226 150 BLs.

227 The characteristic peaks of CH and P-CNF grow proportionally with the number of deposited BL,
228 as observed for neat components the most intense peak is found in the 1100-1000 cm^{-1} region and is
229 ascribed to C-O-C stretching vibration of the glycosidic linkage. This latter peak is centered at 1060
230 cm^{-1} indicating a major contribution from P-CNF. The presence of CH is evidenced by NH_3^+ signals
231 at 1640 and 1540 cm^{-1} (Figure 2 b); it is worth mentioning that such signals are shifted to higher
232 wavenumbers with respect to pure CH (*compare* Figure S1) as a consequence of the ionic
233 interactions established with the negatively charged phosphate groups. The intensity of the peak at
234 1060 cm^{-1} reveals a linear growth for this CH/P-CNF assembly. This signal increases more steeply
235 after the deposition of P-CNF thus indicating this latter as being the main component of the coating.

236 The LbL build-up has also been studied in situ by QCM-D measurements and Figure 2 d reports the
237 shift in normalized resonance frequency (3^{rd} overtone) and energy dissipation as a function of time
238 for the sequential adsorption of CH and P-CNF onto the silicon oxide substrate up to 5 BL. A
239 decrease in resonance frequency indicates adsorption while an increase may refer to desorption of
240 solid material or a change in the solvent content of the adsorbed layer. (Aulin et al., 2008) A steady
241 multilayer film build-up is illustrated by the step-wise decrease in frequency values with P-CNF
242 adsorption being significantly higher than CH, in agreement with IR results. This may be explained
243 by the lower charge density of P-CNF compared to CH (545 *vs*. 6740 μeq/g respectively) where less
244 amount of chitosan is required to neutralize the negatively charged phosphorylated
245 fibrils.(Schlenoff, Ly, & Li, 1998) The LbL assembly is associated with a rather low energy
246 dissipation implying the formation of rather thin and rigid layers. (Ghanadpour, Carosio, &
247 Wågberg, 2017) The amount of adsorbed mass on the QCM crystal upon each layer deposition

calculated using Eq. 1 is reported in Figure 2 e. As expected, the increase in mass is higher due to P-CNF adsorption, which again is in agreement with IR results and indeed reveals the dominance of the phosphorylated fibrils within the formed multilayer film. FE-SEM observations performed for the cross sections of a 150 BL coating deposited on Si wafer highlight the dense and compact nature of this assembly (Figure 2 f). CH acts as continuous matrix embedding P-CNF nanofibrils that are clearly visible at high magnifications.

3.2 Coating assembly on PU foams, morphology, mechanical and flame retardant properties

Following the results described in the previous section, 5BLs of CH/P-CNF assembly have been deposited on PU foams. Low and high magnification FE-SEM observation of neat and LbL-coated foams are reported in Figures S2 and 3, respectively.

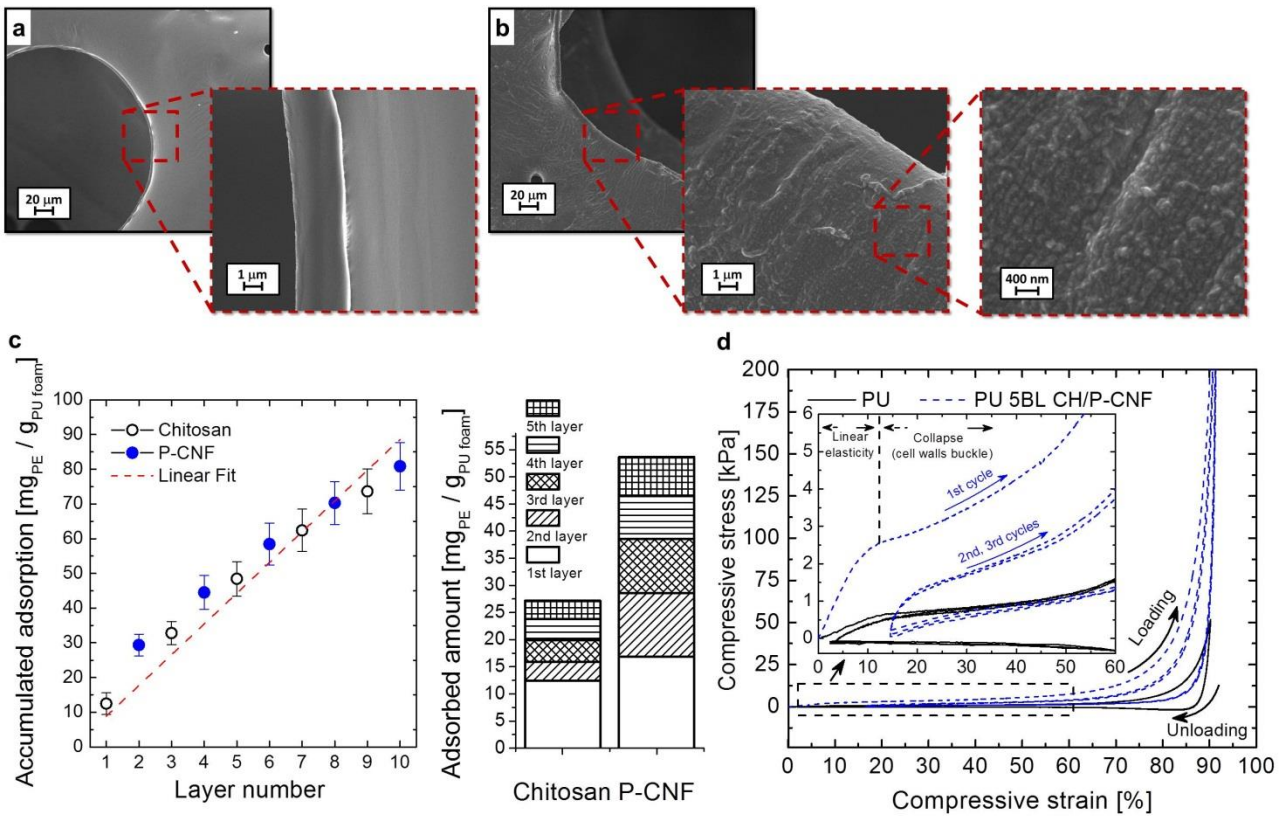

Figure 3. Summary of the LbL treatments of PU foams shown as FE-SEM micrographs of uncoated (a) and LbL-coated (b) PU foams, (c) amount adsorbed on PU foam at each deposition

step evaluated by polyelectrolyte titration and (d) compression tests on uncoated and LbL-coated foams.

The neat PU foam shows a characteristic open cell structure with walls characterized by a smooth and even morphology (Figures S2 a and 3 a). Such morphology is clearly changed by the LbL deposition. Indeed, coated PU clearly shows the formation of a thin and homogeneous coating that extends through the complex 3D structure of the foam. High magnification micrographs clearly demonstrates the nanotexture of the assembly that, similarly to what observed on model Si wafer (Figure 2 f), consist of P-CNF embedded within a CH matrix. From morphological observation it is apparent that the deposited LbL coating results in a continuous and thin exoskeleton that follows the PU structure, easily conforming at the edges of the cell walls without altering its open cell nature (Figure S2). Polyelectrolyte titration was employed in order to evaluate the adsorbed amount of the coating constituents on PU foam after each deposition step; the plot reported in Figure 3 c clearly points out a linear growth where the adsorption of P-CNF results in a more steep increase in mass with respect to CH, especially for the initial layers of the coating. The evaluation of the total adsorbed mass on PU foam (Figure 3 c) indicates an average add-on of 8 wt.-% after 5 BLs with P-CNF as the main component of the coating (66 wt.-%). These results corroborate what observed on model Si and quartz surface by IR spectroscopy and QCM-D measurements, respectively (Figures 2 c and 2 e). The effect of the coating on the foam mechanical properties has been evaluated by compression testing. Figure 3 d shows the stress-strain curve for three subsequent compression cycles performed with the unmodified and the LbL-coated foams. When the foam is compressed, the resulting stress-strain curve normally shows three regions. At low strains, the foam deforms in a linear-elastic way; then, there is a plateau of deformation at almost constant stress, followed by a region of densification where the stress quickly increases as the cell walls crush together. Upon unloading the foam recovers the shape by returning to the original dimensions and shape. The unmodified PU follows this trend during three loading/unloading cycles. A similar behavior can be observed for the LbL-treated foams; however, as reported in Figure 3 d and its inset, the loading

stress values are higher than for the unmodified foam and, after the first compression, the foam is capable of recovering only a fraction of deformation. A similar behavior has been already observed for LbL-treated foams and is ascribed to the effect of the first cycle that by exerting a compression stress on the freshly deposited coating forces its compliance with the PU deformation. (Li, Kim, Shields, & Davis, 2013) This induces the formation of small cracks in the LbL coating and reduces its stiffness thus allowing, during subsequent cycles, for a typical hysteresis curve with a complete recovery of the deformation. Further cycles do not alter the mechanical properties of the coated foams as demonstrated by the second and the third cycles that lay overlapped. This can be also appreciated by observing the data showing the compressive stress as a function of time (Figure S3). The higher stress values required to deform the foam indicate that the first cycle only partially reduces the stiffness of the LbL coating that maintains a good adhesion to the foam and results in a firmer foam. These results further indicate the homogeneity of the coating that, being deposited on each available surface, is capable of modifying the mechanical properties of the foam while maintaining its flexibility. Thanks to the ionic interactions occurring at molecular scale within the LbL assembly and the high strength of the fibrils this CH/P-CNF coating is capable of modifying the PU mechanical properties with only 8 wt.-% of mass added. (Ghanadpour et al., 2017)

3.3 Evaluation of the effect of the LbL coating on flame retardant properties of the PU foams

Treated and untreated PU foams have been subjected to flammability (reaction to a direct flame application) and cone calorimetry (exposure to a heat flux) tests. Both tests represent complementary approaches capable of evaluating the efficiency of the coating in reducing the well-known fire threat of PU foams. Figure 4 summarizes data from flammability and cone calorimetry tests; for the latter, HRR plots as a function of time for untreated and LbL-treated PU is reported. Table 1 collects the complete sets of cone calorimetry data.

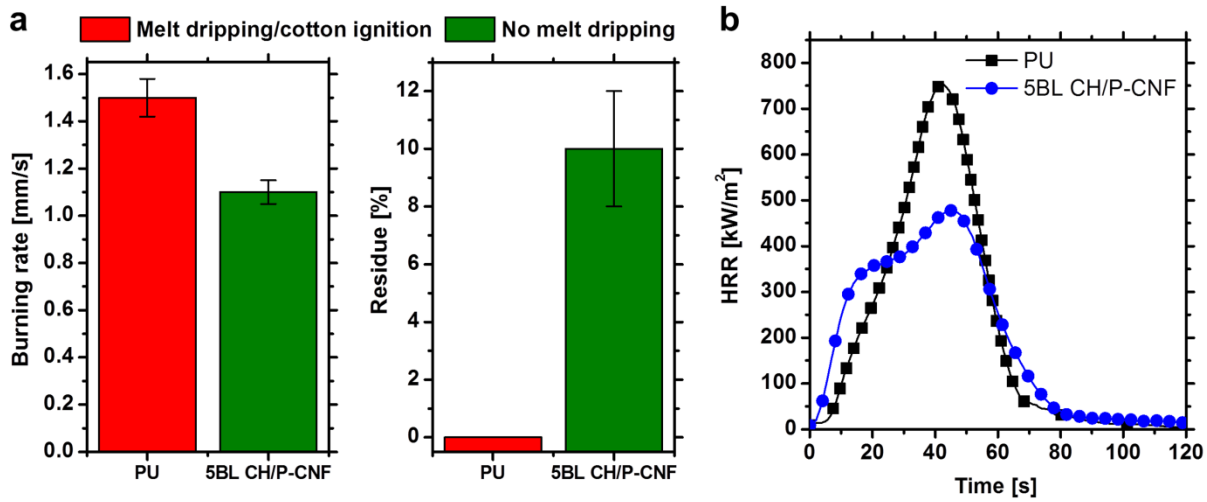

Figure 4. Burning rates and final residues evaluated by flammability tests in horizontal configuration (a) and heat release rate (HRR) plots as function of time measured by cone calorimetry tests (b).

Table 1. Cone calorimetry data of untreated and LbL-treated PU foams.

Sample	TTI ± σ [s]	Av. HRR ± σ [kW/m²]	pkHRR ±σ [kW/m²]	THR ± σ [MJ/m²]	TSR ± σ [m²/m²]	Residue ± σ [%]
PU	11 ±7	154 ± 21	718 ± 70	24.3 ± 0.6	430 ± 13	6 ± 1
5 BL CH/P-CNF	9 ±1	136 ± 11	494 ± 20	23.6 ± 0.5	470 ± 30	7 ± 1

As far as flammability is concerned, upon flame application, the unmodified foam quickly ignites and vigorously burns with flame spreading (1.5 mm/s) to the entire length of the sample. During combustion the foam melts and collapses releasing droplets of burning molten polymer that ignite the dry cotton placed underneath the sample. This behavior, known as melt-dripping, represents one of the most severe safety threat of PU foams as it can easily spread the fire to other ignitable materials leading to dangerous flashover events. Conversely, LbL-coated PU foams showed a completely different burning behavior. Upon ignition a small flame slowly propagates (1.1 mm/s) on the samples leaving a charred residue behind. The melt dripping is completely suppressed and, although the flame spread to the entire length of the sample, at the end of the test it is possible to

collect a coherent residue accounting for 10% of the original mass. This points out that the flame self-extinguished before being able to completely consume the PU. From an overall point of view, LbL-treated PU foams show an improved behavior due to the formation of a protective coating that prevents foam collapse and limits the release of combustible volatiles consistently reducing the burning rate. This completely suppresses melt dripping but does not allow for the self-extinguishing of the flame before it spreads to entire length of the specimen. Cone calorimetry tests (Figure 4 b) have been performed using a heat flux of 35 kW/m^2 corresponding to a fire in the developing stages. (Schartel & Hull, 2007) Upon exposure to the heat flux the unmodified PU starts degrading, releasing combustible volatile gases that lead to sample ignition and flaming combustion. During combustion the foam collapses forming a pool of a low viscosity liquid simultaneously reaching the maximum heat release rate (718 k/m^2).(Kramer, Zammarano, Linteris, Gedde, & Gilman, 2010) This behavior has been demonstrated to be very dangerous as it increases the flame spread rate by boosting the combustion rate of other burning items. On the other hand, for the foam coated with 5 BL it is possible to observe the formation of a char layer that quickly extends to the entire foam and prevents the structure from collapsing. This partially hinders the foam combustion and results in a reduced pkHRR (- 31%). THR and TSR values remain almost unchanged and within the experimental error. The final residue is slightly increased moving from 6 to 7 % for the uncoated and LbL-coated foams, respectively. Similar to what was observed in the flammability tests, such results can be ascribed to the presence of the coating that acts as a barrier controlling the mass and heat exchange between the gas and condensed phase. This reduces the release rate of the volatiles and subsequently results in a reduction of heat release rate parameters.

3.4 Assembly thermal stability and fire shielding ability on PU foams

From the characterization performed on untreated and LbL-treated foams it its quite apparent that the CH/P-CNF nano-exoskeleton is capable of strongly modifying the foam morphologically and mechanically apart from changing its fire properties. This can be ascribed to the homogeneity and

continuous nature of the coating that extends through the entire thickness of the foam covering each available surface. However, although the change in mechanical properties can be explained by the strong ionic interactions among the assembled components, there are no studies trying to explain the improvements in flame retardant properties. Thus, in an effort to further understand the role of the deposited coating, a detailed study of the thermal stability and structural-chemical evolution of CH/P-CNF assembly during combustion has been performed. Figure 5 shows the results collected by TGA under nitrogen atmosphere for neat CH, neat P-CNF and a LbL-assembled CH/P-CNF model consisting of 150 BL. In addition, the morphological and chemical changes in such LbL coating deposited on Si wafer following exposure to 35 kW/m^2 heat flux are displayed.

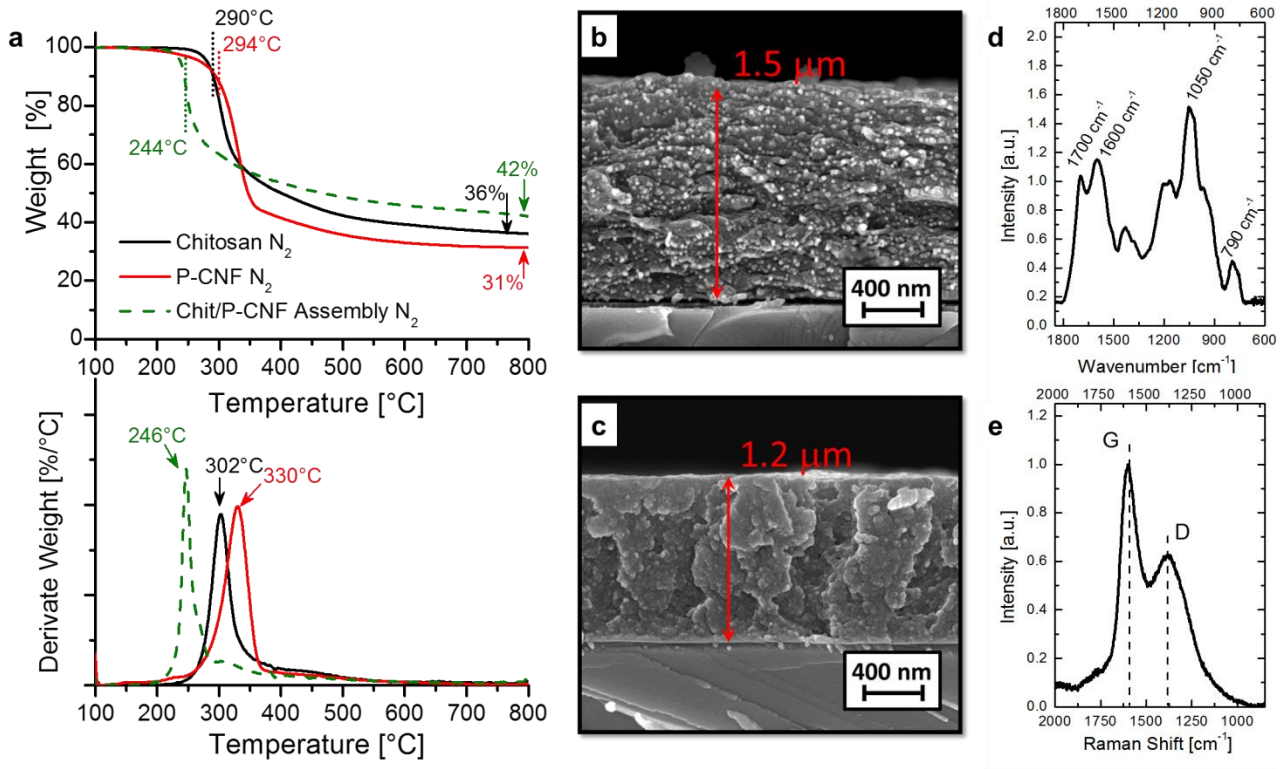

Figure 5. TG and dTG curves of neat and LbL-assembled components under nitrogen atmosphere (a), FE-SEM micrographs of the coating cross section before (b) and after (c) exposure to 35 kW/m^2, IR (d) and Raman (e) spectra of the coating after exposure to 35 kW/m^2.

TGA performed under nitrogen atmosphere simulate the pyrolysis that occurs in the condensed phase during combustion owing to essentially anaerobic atmosphere under the surface of the

burning material. First of all the neat components have been evaluated. Both CH and P-CNF degrade with a well-defined single step that occurs between 250-400°C. As well documented in the literature during this step CH releases H_2O, NH_3, CO, CO_2 and CH_3COOH and forms a carbonaceous residue that subsequently undergoes a slow and continuous modification, with the production of CH_4, towards polyaromatic structures (final residue 36%).(Pawlak & Mucha, 2003) (Corazzari et al., 2015) The P-CNF follows characteristic degradation path of cellulose; however, thanks to the char promoting action of the phosphorylation functionalization, the amount of charred residue produced at the end of the first step and at 800°C is consistently higher (31%) than what normally reported for cellulose or non-phosphorylated CNF. (J. Alongi, Camino, & Malucelli, 2013) (Ghanadpour et al., 2015) When the two components are LbL-assembled, the resulting material still shows a single step thermal degradation that is anticipated at 244°C, as reported in Figure 5 a. This can be related to the phosphate groups of P-CNF and, although an earlier degradation may be considered a detrimental effect, it allows the CH/P-CNF coating to promptly react to a temperature raise and produce a thermally stable residue/barrier. Moreover, the resulting thermal stability is unexpectedly higher than that of the pure CH and P-CNF as clearly pointed out by the weight curve that remains above the region associated to any theoretical mixture of non-interacting components. This can be ascribed to the achieved intimate and a stoichiometric assembly of the two components into a material characterized by strong ionic intermolecular interactions. The residue produced after the first step is 70% while the final residue is as high as 42 %. The same CH/P-CNF assembly deposited as 150 BL coating on model Si wafer surface, has been exposed to the cone heat flux (the same adopted during the tests on foams) and then imaged with FE-SEM and analyzed by ATR-IR and Raman spectroscopy. FE-SEM observations clearly point out a structural change in the coating that is not destroyed by the heat flux but, as studied by TGA, evolves towards the formation of a charred dense structure with a 25% reduction in thickness. ATR spectroscopy suggests the formation of an aromatic carbonaceous structure (signal at 1600 cm^{-1} ascribed to aromatic C=C stretching); in addition, the presence of carboxyl groups (1700 cm^{-1}) and

only one peak in the 900-700 cm^{-1} region (790 cm^{-1}, ascribed to out of plane C-H vibration in substituted aromatic rings) suggest the formation of aromatic structures with different degrees of substitution. (Soares, Camino, & Levchik, 1995) (Socrates, 2006) A strong signal found at 1050 cm^{-1} can be related to P-O-C or P-N-C bonds indicating the condensed char promoting action of the phosphorylation functionalization. Raman spectroscopy provides information regarding the quality of the produced aromatic char that can be related to its thermal stability. (Carosio & Alongi, 2016a) Two characteristic signals, known as G and D bands, associated to polyaromatic hydrocarbons are clearly visible at 1590 and 1350 cm^{-1}. (Ferrari & Basko, 2013) The presence of the D band, normally associated to defects, corroborates ATR-IR information; however, the fact that this latter band is clearly less intense than the G band indicates the graphitic-like structure of the barrier produced by the thermal degradation of the CH/P-CNF assembly.

It is apparent that the favored char forming ability of the CH/P-CNF assembly represents a key-point in the flame retardant activity of the coating. In order to investigate whether this behavior is maintained also when the coating is deposited on PU foams, small (1x1x1 cm^3) species of uncoated and coated foams have been exposed to the cone heat flux and then imaged by FE-SEM. Figure 6 summarizes a number of collected snapshots and corresponding micrographs.

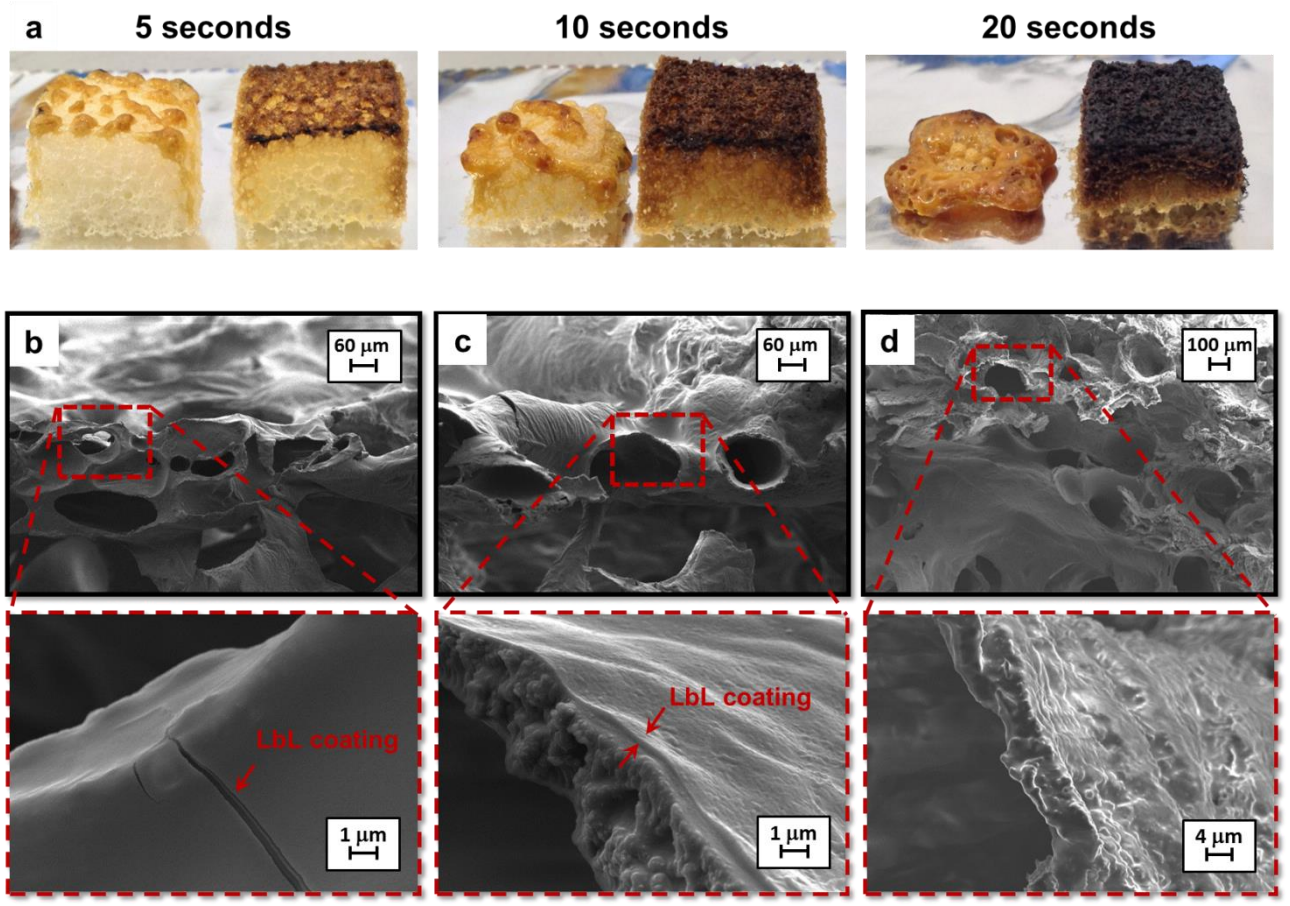

Figure 6. Digital images of uncoated and LbL-coated PU foams after exposure to 35 kW/m^2 (a) and FE-SEM micrographs of LbL-coated PU foam exposed to 35 kW/m^2 for 5 (b), 10 (c) and 20 (d) seconds.

The snapshots clearly point out an extensive char formation for the coated PU foam. This starts from the top surface and is extended to the entire structure within 20 seconds. During the same time, the uncoated foam completely melts and collapses. From FE-SEM micrographs it is possible to observe the presence of a protective char layer on the surface of PU foam. This thin charred layer is still visible even after 10 seconds of exposure while after 20 seconds it is embedded within the melting PU. On the basis of the above observations and the coating thermal degradation it is possible to formulate a mechanism of action for the deposited CH/P-CNF assembly. Upon exposure to a flame or a heat flux the coating constituents start degrading, building protective layers characterized by a graphitic like structure. This occurs at low temperatures (around 240 °C) and

produces a compaction in the coating thickness as evidenced by TG and FE-SEM observations on the LbL assembled CH/P-CNF (Figure 5). Such char forming interaction is enhanced by the ionic linkages and the intimate contact established during the LbL assembly which allows for synergistic interactions between the phosphate groups of P-CNF and the protonated amine of CH. In this way the coating can quickly and efficiently evolve towards thermally stable polyaromatic structures that, being located at the interface between the condensed and the gas phase, can exert a flame retardant effect. Indeed, the so produced charred exoskeleton acts as a barrier to heat and volatile release while mechanically sustaining the foam that would otherwise collapse. It is important to highlight the importance of this latter effect as a thin charred layer having a high mechanical stiffness which sustains and supports the foamed structure. These two combined effects allow for the suppression of melt dripping while also strongly affecting volatile release rates thus producing the observed reduction in pkHRR and avHRR values.

4. Conclusions

This paper shows extensive results from layer-by-layer assembled nanostructured thin films based on CH and P-CNF to be used as a flame retardant exoskeleton for PU foams. The build-up of the nanostructured films follows a linear growth regime where the phosphorylated nanocellulose component represents the major fraction of the final assembly. A unique nanostructure comprising phosphorylated nanofibrils embedded within a CH continuous matrix is obtained as demonstrated by field emission scanning electron microscopy. This assembly can be easily deposited on open cell polyurethane foams yielding a submicron exoskeleton capable of covering the complex 3D structure of the foam without altering its open cell nature. Compression test demonstrated that the LbL deposition is capable of improving the mechanical properties of the foam while maintaining its characteristic flexibility. This occurs with only 8% of coating mass added and has been ascribed to the nanostructure of the assembly and the strong ionic interaction occurring at the molecular scale between the assembled CH and P-CNF. From the flame retardancy point of view, coated foams

were able to suppress melt dripping during flammability tests and reducing the combustion rate by 31% as evaluated by cone calorimetry testing. The mechanism behind the flame retardant effect of the deposited coating has been thoroughly analyzed and correlated with the coating composition and the achieved results. When exposed to a heat flux (or a flame) the coating constituents undergo a favorable degradation pathway that results in the build-up of thermally stable aromatic structures that act as protective barrier towards heat and flammable volatile release. The produced charred barrier also displays impressive mechanical properties as it is capable of mechanically sustaining the foam during combustion preventing its collapse. This is achieved thanks to the unique structure imparted by the layer-by-layer assembly that during thermal degradation favors synergistic rather than simply additive interactions between the two components. This paper allows for a further step towards the efficient use of sustainable resources for the LbL construction of functional flame retardant materials and poses the base for a deeper insight and a better understanding of the structure to properties relationship in FR-LbL assemblies.

Acknowledgements

The authors want to thank Mr. Mauro Raimondo for FE-SEM analyses and Mr. Fabio Cuttica for cone calorimetry tests. In addition, the authors would like to acknowledge the FireFoam project funded by SSF (RMA11-0065) in Sweden and Lars Wågberg acknowledges Wallenberg Wood Science Centre for financing.

References

Alongi, J., Camino, G., & Malucelli, G. (2013). Heating rate effect on char yield from cotton, poly(ethylene terephthalate) and blend fabrics. *Carbohydr Polym,* 92(2), 1327-1334.

Alongi, J., Carletto, R. A., Di Blasio, A., Cuttica, F., Carosio, F., Bosco, F., & Malucelli, G. (2013). Intrinsic intumescent-like flame retardant properties of DNA-treated cotton fabrics. *Carbohydr Polym,* 96(1), 296-304.

Alongi, J., Cuttica, F., & Carosio, F. (2016). DNA Coatings from Byproducts: A Panacea for the Flame Retardancy of EVA, PP, ABS, PET, and PA6? *ACS Sustainable Chemistry & Engineering,* 4(6), 3544-3551.

Alongi, J., Di Blasio, A., Cuttica, F., Carosio, F., & Malucelli, G. (2014). Bulk or surface treatments of ethylene vinyl acetate copolymers with DNA: Investigation on the flame retardant properties. *European Polymer Journal,* 51, 112-119.

Aulin, C., Varga, I., Claesson, P. M., Wågberg, L., & Lindström, T. (2008). Buildup of polyelectrolyte multilayers of polyethyleneimine and microfibrillated cellulose studied by in situ dual-polarization interferometry and quartz crystal microbalance with dissipation. *Langmuir,* 24(6), 2509-2518.

Cain, A. A., Plummer, M. G. B., Murray, S. E., Bolling, L., Regev, O., & Grunlan, J. C. (2014). Iron-containing, high aspect ratio clay as nanoarmor that imparts substantial thermal/flame protection to polyurethane with a single electrostatically-deposited bilayer. *Journal of Materials Chemistry A,* 2(41), 17609-17617.

Carosio, F., & Alongi, J. (2016a). Influence of layer by layer coatings containing octapropylammonium polyhedral oligomeric silsesquioxane and ammonium polyphosphate on the thermal stability and flammability of acrylic fabrics. *Journal of Analytical and Applied Pyrolysis,* 119, 114-123.

Carosio, F., & Alongi, J. (2016b). Ultra-Fast Layer-by-Layer Approach for Depositing Flame Retardant Coatings on Flexible PU Foams within Seconds. *Acs Applied Materials & Interfaces,* 8(10), 6315-6319.

Carosio, F., Alongi, J., & Malucelli, G. (2012). Layer by Layer ammonium polyphosphate-based coatings for flame retardancy of polyester–cotton blends. *Carbohydr Polym,* 88(4), 1460-1469.

Carosio, F., Cuttica, F., Di Blasio, A., Alongi, J., & Malucelli, G. (2015). Layer by layer assembly of flame retardant thin films on closed cell PET foams: Efficiency of ammonium polyphosphate versus DNA. *Polymer Degradation and Stability,* 113, 189-196.

Carosio, F., Kochumalayil, J., Cuttica, F., Camino, G., & Berglund, L. (2015). Oriented clay nanopaper from biobased components--mechanisms for superior fire protection properties. *ACS Appl Mater Interfaces,* 7(10), 5847-5856.

Cho, J. H., Vasagar, V., Shanmuganathan, K., Jones, A. R., Nazarenko, S., & Ellison, C. J. (2015). Bioinspired catecholic flame retardant nanocoating for flexible polyurethane foams. *Chemistry of Materials,* 27(19), 6784-6790.

Corazzari, I., Nisticò, R., Turci, F., Faga, M. G., Franzoso, F., Tabasso, S., & Magnacca, G. (2015). Advanced physico-chemical characterization of chitosan by means of TGA coupled on-line with FTIR and GCMS: Thermal degradation and water adsorption capacity. *Polymer Degradation and Stability,* 112, 1-9.

Dash, M., Chiellini, F., Ottenbrite, R. M., & Chiellini, E. (2011). Chitosan—A versatile semi-synthetic polymer in biomedical applications. *Progress in Polymer Science,* 36(8), 981-1014.

Decher, G. (1997). Fuzzy nanoassemblies: Toward layered polymeric multicomposites. *Science,* 277(5330), 1232-1237.

Du, X., Zhang, Z., Liu, W., & Deng, Y. (2017). Nanocellulose-based conductive materials and their emerging applications in energy devices-A review. *Nano Energy*.

Ferrari, A. C., & Basko, D. M. (2013). Raman spectroscopy as a versatile tool for studying the properties of graphene. *Nat Nano,* 8(4), 235-246.

Ghanadpour, M., Carosio, F., Larsson, P. T., & Wagberg, L. (2015). Phosphorylated cellulose nanofibrils: a renewable nanomaterial for the preparation of intrinsically flame-retardant materials. *Biomacromolecules,* 16(10), 3399-3410.

Ghanadpour, M., Carosio, F., & Wågberg, L. (2017). Ultrastrong and flame-resistant freestanding films from nanocelluloses, self-assembled using a layer-by-layer approach. *Applied Materials Today,* 9, 229-239.

Hammel, S. C., Hoffman, K., Lorenzo, A. M., Chen, A., Phillips, A. L., Butt, C. M., . . . Stapleton, H. M. (2017). Associations between flame retardant applications in furniture foam, house dust levels, and residents' serum levels. *Environment international,* 107, 181-189.

Henriksson, M., Berglund, L. A., Isaksson, P., Lindstrom, T., & Nishino, T. (2008). Cellulose nanopaper structures of high toughness. *Biomacromolecules,* 9(6), 1579-1585.

Hirschler, M. M. (2008). Polyurethane foam and fire safety. *Polymers for Advanced Technologies,* 19(6), 521-529.

Jorfi, M., & Foster, E. J. (2015). Recent advances in nanocellulose for biomedical applications. *Journal of Applied Polymer Science,* 132(14).

Klemm, D., Kramer, F., Moritz, S., Lindstrom, T., Ankerfors, M., Gray, D., & Dorris, A. (2011). Nanocelluloses: a new family of nature-based materials. *Angew Chem Int Ed Engl,* 50(24), 5438-5466.

Koklukaya, O., Carosio, F., & Wãgberg, L. (2017). Superior Flame-Resistant Cellulose Nanofibril Aerogels Modified with Hybrid Layer-by-Layer Coatings. *Acs Applied Materials & Interfaces,* 9(34), 29082-29092.

Kramer, R. H., Zammarano, M., Linteris, G. T., Gedde, U. W., & Gilman, J. W. (2010). Heat release and structural collapse of flexible polyurethane foam. *Polymer Degradation and Stability,* 95(6), 1115-1122.

Lavoine, N., Desloges, I., Dufresne, A., & Bras, J. (2012). Microfibrillated cellulose - its barrier properties and applications in cellulosic materials: a review. *Carbohydr Polym,* 90(2), 735-764.

Leistner, M., Abu-Odeh, A. A., Rohmer, S. C., & Grunlan, J. C. (2015). Water-based chitosan/melamine polyphosphate multilayer nanocoating that extinguishes fire on polyester-cotton fabric. *Carbohydr Polym,* 130, 227-232.

Li, Y. C., Kim, Y. S., Shields, J., & Davis, R. (2013). Controlling polyurethane foam flammability and mechanical behaviour by tailoring the composition of clay-based multilayer nanocoatings. *Journal of Materials Chemistry A,* 1(41), 12987-12997.

Liu, A., & Berglund, L. A. (2012). Clay nanopaper composites of nacre-like structure based on montmorrilonite and cellulose nanofibers—improvements due to chitosan addition. *Carbohydr Polym,* 87(1), 53-60.

Pawlak, A., & Mucha, M. (2003). Thermogravimetric and FTIR studies of chitosan blends. *Thermochimica Acta,* 396(1), 153-166.

Rodahl, M., Höök, F., Krozer, A., Brzezinski, P., & Kasemo, B. (1995). Quartz crystal microbalance setup for frequency and Q-factor measurements in gaseous and liquid environments. *Review of Scientific Instruments,* 66(7), 3924-3930.

Schartel, B., & Hull, T. R. (2007). Development of fire-retarded materials—Interpretation of cone calorimeter data. *Fire and Materials,* 31(5), 327-354.

Schlenoff, J. B., Ly, H., & Li, M. (1998). Charge and mass balance in polyelectrolyte multilayers. *Journal of the American Chemical Society,* 120(30), 7626-7634.

Soares, S., Camino, G., & Levchik, S. (1995). Comparative-Study of the Thermal-Decomposition of Pure Cellulose and Pulp Paper. *Polymer Degradation and Stability,* 49(2), 275-283.

Socrates, G. (2006). *Infrared and Raman Characteristic Group Frequencies - Table and Charts*. (third edition ed.): Wiley.

Stieger, G., Scheringer, M., Ng, C. A., & Hungerbuhler, K. (2014). Assessing the persistence, bioaccumulation potential and toxicity of brominated flame retardants: Data availability and quality for 36 alternative brominated flame retardants. *Chemosphere,* 116, 118-123.

Xu, D., Yu, K., & Qian, K. (2017). Effect of tris (1-chloro-2-propyl) phosphate and modified aramid fiber on cellular structure, thermal stability and flammability of rigid polyurethane foams. *Polymer Degradation and Stability,* 144, 207-220.